JOURNAL OF AIRCRAFT
Vol. 46, No. 6, November–December 2009

Engineering Notes

Efficient Aeroelastic Analysis Method Including Inverse Design for Body Effects

Seung-Jun Lee,* Dong-Kyun Im,* Myung-Koo Kang,*
In Lee,† and Jang-Hyuk Kwon‡
Korea Advanced Institute of Science and Technology, Daejeon 305-701, Republic of Korea

DOI: 10.2514/1.43669

Nomenclature

$[C_g]$	=	generalized damping matrix
C_p	=	pressure coefficient
C_r	=	root chord length
F_i	=	positive constants, $i = 0$–2.
$[K_g]$	=	generalized stiffness matrix
M	=	freestream Mach number
$[M_g]$	=	generalized mass matrix
$\{Q\}$	=	generalized aerodynamic force vector
$\{q\}$	=	generalized modal displacement vector
R	=	pressure difference between target and baseline airfoil
S	=	area of the lifting surface or airfoil geometry
t	=	time, nondimensionalized by U/c_r
U	=	freestream velocity
$\{u\}$	=	physical displacement vector
x, y, z	=	nondimensional physical coordinates in the streamwise, spanwise, and vertical directions
γ	=	specific heat ratio
ΔC_p	=	difference of the lifting pressure coefficients between the upper and lower lifting surfaces
ρ	=	freestream density
ϕ	=	disturbance velocity potential
$[\psi]$	=	modal matrix

I. Introduction

AEROELASTICITY is the research field of studying the interaction between the structural dynamics and aerodynamics. It deals with the complex coupled phenomena of aircraft in extreme flight conditions in the design stage of aircraft development. Among the aeroelastic problems, flutter phenomenon is the most dangerous one. Furthermore, if the aircraft flies in the transonic range, the aerodynamic complexity resulting from shock wave oscillation, flow separation, and so forth, dramatically increases. Therefore, the investigation of nonlinear aerodynamics based on computational fluid dynamics (CFD) has become important in recent aeroelastic analysis. An aeroelastic examination using an efficient unsteady aerodynamic analysis with the transonic small-disturbance (TSD) equation, which has been widely recognized as one of the most efficient CFD-based approaches, has especially strong computational advantages in many different types of parametric studies, because TSD code does not require CFD grid regeneration but only changes in wing surface slope due to structural motion on a fixed-grid system [1]. Based on these advantages, full-span aircraft have been studied. In an active way, the fuselage is usually represented by a box within the embedded multigrid. Instead of the former method, the CFD-based aeroelastic analysis of a complex full-span aircraft model has been performed by Yoo et al. [2] assuming that the aerodynamics of a wing are not influenced by the body shape. This assumption is meaningful from an aeroelastic point of view, because the main part of lift and flexibility is contributed by the wing. Nevertheless, the fuselage can distort the aerodynamic small-disturbance pressure on the wing surface, and it is necessary to investigate the body effect in flutter analysis [3].

To compute a pressure perturbation due to the fuselage, an inverse design method is applied in this research. A typical inverse design method is mainly used to automatically optimize the airfoil geometry to the level of an adequate target pressure. There are several kinds of inverse design methods, such as the MGM (modified Garabedian–McFadden) method [4], defection correction method [5], spring-analogy traction method [6], free-form deformation method, and so on. Among them, the MGM method is simple and easy to adopt because it uses only one auxiliary equation to obtain the target airfoil shape. This simplicity can be effective for the CFD-based aeroelastic analysis problems, which need a tremendous computing time. The MGM method assumes that the pressure difference between target and baseline airfoils is a function of surface displacement and its first and second derivatives. The MGM auxiliary equation regards the rate of change in surface slope as a pseudotime term and iterates until it converges to zero.

Figure 1 shows the flowchart of inverse design procedure. As with the other CFD analysis process, the grid is generated first. Next, the steady aerodynamics are analyzed. Then the pressure distribution on a wing surface is compared with the target pressure distribution. If the residual term is not zero, all the steps are repeated. However, the main advantage is in the loop. Unlike other CFD codes, the TSD-based aeroelastic code does not require grid regeneration for every step. It proceeds with information on surface slope variation.

In this study, an efficient aeroelastic analysis method including body aerodynamics is introduced. First, TSD theory and aeroelastic equation are explained briefly. Next, the MGM inverse design method is used to modify the aerodynamic force to include the body effect. In sequence, the validation of the MGM method is given. Then the wing-body model is selected as a numerical example. Finally, the modified aeroelastic analysis follows.

II. Theoretical Background

A. Unsteady TSD Equation

The complex transonic flowfield can be solved by the Navier–Stokes theory. The resulting nonlinear aerodynamic equations are the most accurate, but this solution may require a large amount of computing time. Proper assumptions such as inviscid, irrotational, and small-perturbation hypothesis lead the Navier–Stokes equations to the TSD equations. The TSD theory is powerful when it is applied to an airfoil with small thickness. A three-dimensional unsteady TSD equation is written in conservation-law form as follows [7]:

$$\frac{\partial f_0}{\partial t} + \frac{\partial f_1}{\partial x} + \frac{\partial f_2}{\partial y} + \frac{\partial f_3}{\partial z} = 0 \tag{1}$$

Received 6 February 2009; revision received 12 July 2009; accepted for publication 21 July 2009.

*Graduate Research Assistant, Department of Aerospace Engineering, 335 Gwahangno, Yuseong-gu.
†Professor, Department of Aerospace Engineering, 335, Gwahangno, Yuseong-gu. AIAA Associate Fellow (Corresponding Author).
‡Professor, Department of Aerospace Engineering, 335, Gwahangno, Yuseong-gu.

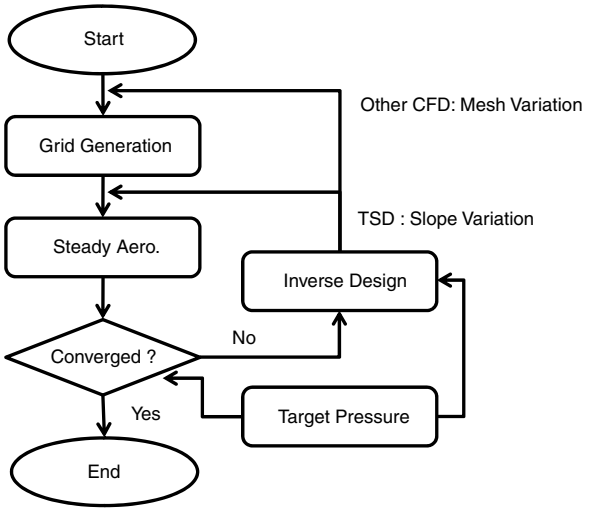

Fig. 1 Flowchart of inverse design method combined with CFD analysis procedure.

where

$$f_0 = -A\phi_t - B\phi_x \qquad f_1 = E\phi_x + F\phi_x^2 + G\phi_y^2$$
$$f_2 = \phi_y(1 + H\phi_x) \qquad f_3 = \phi_z$$

Here, t and x, y, and z are nondimensionalized by U/c_r and c_r, respectively. The coefficients A, B, E, F, G, and H are determined by the freestream Mach number M and the specific heat ratio γ. The coefficients can be chosen depending upon the assumptions used when deriving the TSD equation [1]. The coefficients defined by NASA Ames Research Center are presented in [8]. Equation (1) was reformulated by Batina [7] by using a time-accurate AF (approximate factorization) algorithm, which consists of a time linearization procedure coupled with a Newton iteration technique [9]. An Engquist–Osher scheme is used in the AF algorithm to get numerical stability, and nonreflecting far-field boundary condition is applied.

B. Aeroelastic Equation of Motion

For computational efficiency, the aeroelastic equation is arranged with the modal transformation [8]:

$$[M_g]\{\ddot{q}\} + [C_g]\{\dot{q}\} + [K_g]\{q\} = \{Q(t, q, \dot{q})\} \tag{2}$$

Thus, Eq. (2) is the generalized aeroelastic equation of motion, and $\{Q\}$, the external aerodynamic force vector represented in a generalized coordinate system, is defined by [9]

$$\{Q\} = [\psi]^T \frac{1}{2}\rho U^2 \int_s \Delta C_p \, \mathrm{d}S \tag{3}$$

where $[\psi]$, the mode shape matrix, is splined into a TSD grid from the finite element method grid. For the spline process, an infinite-plane-surface spline method is used. The displacement vector can be expressed as

$$\{u\} = [\psi]\{q\} \tag{4}$$

C. MGM Inverse Design Method

The MGM inverse design method is one of the residual correction methods. This method assumes that the pressure difference between the target and the baseline airfoils correlates with the surface velocity and the first and second derivatives of it:

$$F_0 S_t + F_1 S_{xt} + F_2 S_{xxt} = R \tag{5}$$

where R is the residual, defined as $R = C_p^{\text{target}} - C_p^{\text{baseline}}$. The coefficients F_0, F_1, and F_2 are nonnegative constants that are chosen to provide a stable iterative process [10]. The subscripts t and x mean the pseudotime and streamwise axis, respectively.

Equation (5) is solved by writing the finite difference expression. The upwind method is used for the finite difference of the first derivative term and for the central difference of the second derivative term. As in [4], the time step is set to be 1. Then Eq. (5) is written as

$$A_i \Delta S_{i+1} + B_i \Delta S_i + C_i \Delta S_{i-1} = R_i \tag{6}$$

where the coefficients for the lower and upper surfaces are given next in the left and right columns, respectively [4]:

$$A_i = -\frac{F_1}{x_i - x_{i+1}} - \frac{2F_2}{(x_{i+1} - x_i)(x_{i+1} - x_{i-1})}$$
$$A_i = \frac{2F_2}{(x_{i+1} - x_i)(x_{i+1} - x_{i-1})}$$
$$B_i = F_0 + \frac{F_1}{x_i - x_{i+1}} + \frac{2F_2}{(x_{i+1} - x_i)(x_i - x_{i-1})}$$
$$B_i = F_0 + \frac{F_1}{x_i - x_{i-1}} + \frac{2F_2}{(x_{i+1} - x_i)(x_i - x_{i-1})}$$
$$C_i = \frac{2F_2}{(x_i - x_{i-1})(x_{i+1} - x_{i-1})}$$
$$C_i = \frac{F_1}{x_i - x_{i-1}} - \frac{2F_2}{(x_i - x_{i-1})(x_{i+1} - x_{i-1})}$$
$$R_i = -R_i \qquad R_i = R_i$$

Figure 2 shows the numbering sequence of grid points for an airfoil. Boundary conditions are applied to the leading-edge and trailing-edge regions. In this research, the variation of trailing-edge point is set to be zero and the leading-edge point is determined by the mean of the neighboring points because of the ambiguity of upwind differencing at the leading edge. Finally, Eq. (6), which forms the tridiagonal matrix, is solved by a Thomas algorithm. The temporal geometry is updated by adding the result of a Thomas algorithm.

The MGM method is validated by using a symmetric 2-D airfoil-section test case at a 0 deg angle of attack. Steady aerodynamic analysis is conducted with the TSD code at Mach number 0.7. Figure 3 shows the numerical test results of the MGM method on a symmetric airfoil. The baseline and target airfoil sections are the NACA64A006 and NACA64A010, respectively. Pressure coefficient distribution, airfoil geometry, and airfoil slope information are in Figs. 3a–3c, respectively. The slope data must be computed by the MGM method because the inverse design code is combined with the TSD aeroelastic code.

III. Numerical Results and Discussion

A wing-body model is taken from [11]. The schematic geometry of the NACA RM L51F07 experimental wing-body model is shown in Fig. 4.

Wing aspect ratio is 4 and taper ratio is 0.6. Incidence angle, dihedral angle, and wing twist are all equal to zero. The airfoil section is the NACA65A006 and the wing is swept back by 45 deg. The fuselage cross section is circular and the center is located on the x axis. The longitudinal variation in fuselage radius can be found in [11]. To generate the CFD grid, linear interpolation was used to obtain the value of radius between discrete fuselage geometry data. The wing-body model is symmetric about the x–z plane. The

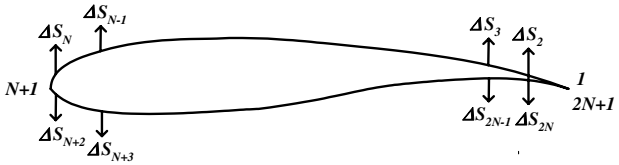

Fig. 2 Numbering order of airfoil grid points for the inverse design method.

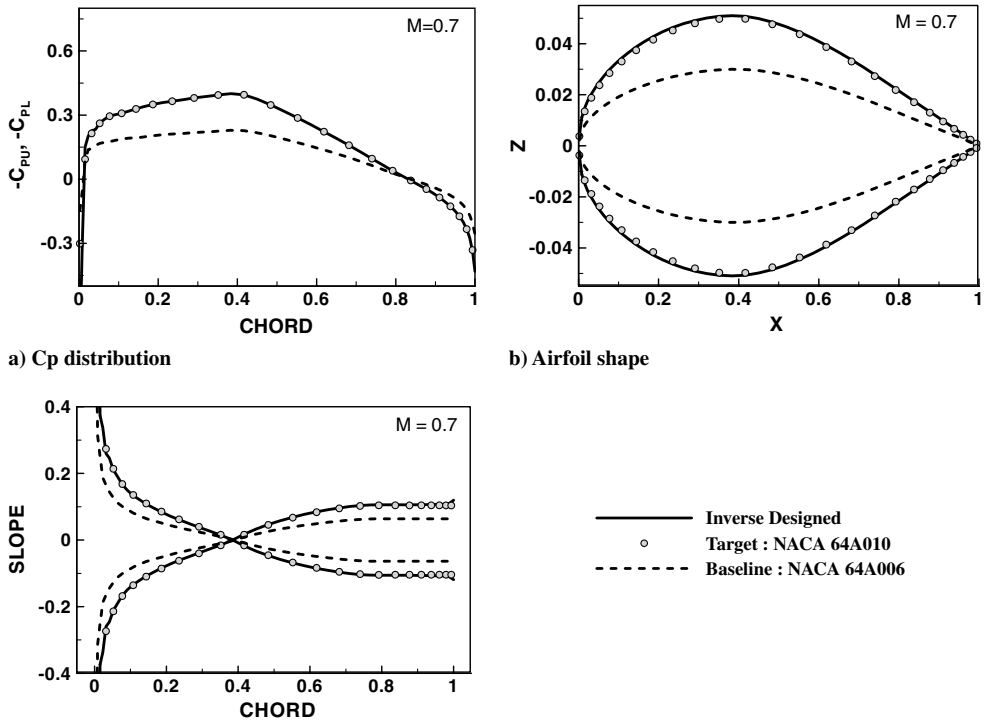

a) Cp distribution

b) Airfoil shape

c) Surface slope

Fig. 3 MGM method validation with 2-D airfoil (baseline: NACA64A006, target: NACA64A010).

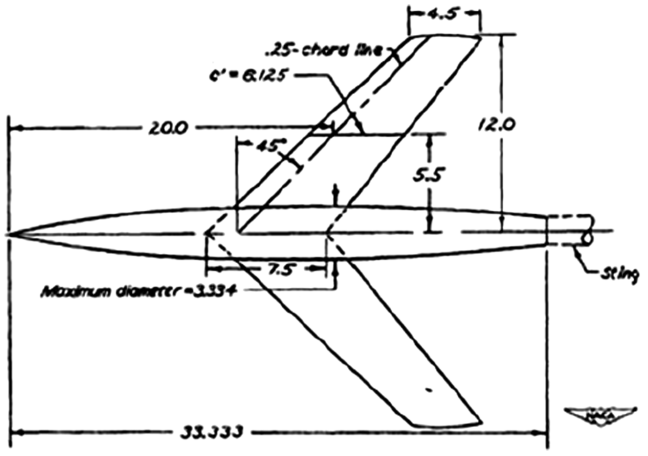

Fig. 4 NACA RM L51F07 experimental wing-body model (dimensions in inch).

fuselage ends with a sting support, designed to attach the model onto the wind-tunnel turntable.

Figure 5 shows the structured Euler grid for the wing-body model. The sting is excluded because its influences on wing aerodynamics are assumed to be negligible. The grid shown in Fig. 5a consists of two H-H-type multiblock grids and the mesh size is $277 \times 451 \times 21$ points. Grid size on the wing surface is 81×49 points. Wing tip is shaped by rotation of the symmetric airfoil section about its chord line with grid lines at five angular positions. The Euler code is used for the analysis of the complete wing-body model. It is based on the cell-centered finite volume method with a second-order total-variation-diminishing scheme. The hyperbolic equations are solved by alternating-direction-implicit and dual-time-stepping methods [12].

Figure 6 shows the TSD grid for the wing-only model. The total grid size is $80 \times 40 \times 40$ points, and 50×30 grid points are on the wing surface. Because the TSD grid is Cartesian, the round wing tip is not modeled.

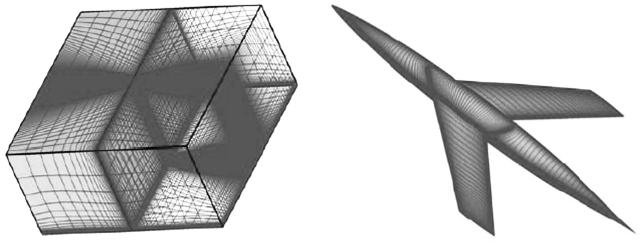

a) H-H type b) Wing-body model

Fig. 5 Euler grid of the wing-body model.

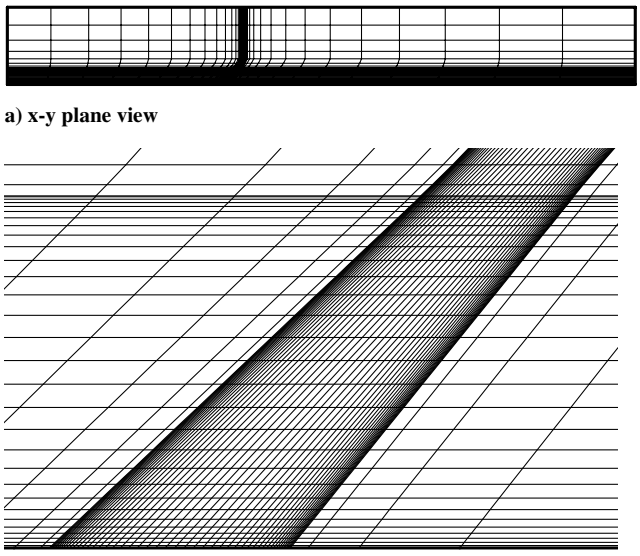

a) x-y plane view

b) Close view of wing surface grid

Fig. 6 TSD grid of the wing model.

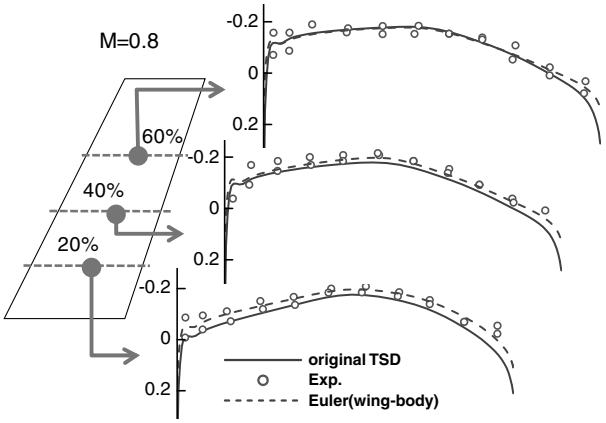

a) Mach 0.8

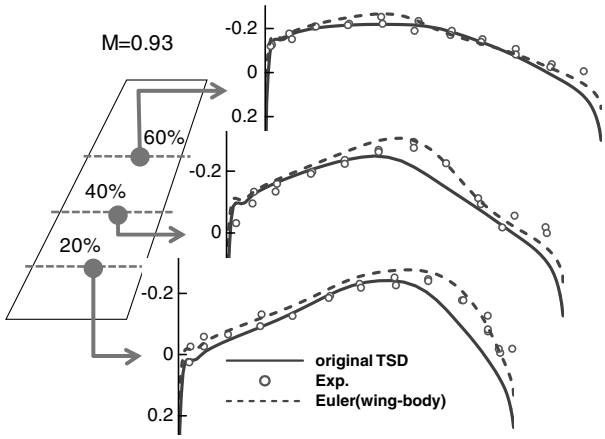

b) Mach 0.93

Fig. 7 Comparison of steady aerodynamics between Euler wing-body model and TSD wing model at $M = 0.8, 0.93$ and angle of attack of 0 deg.

Figure 7 shows the comparison of the steady aerodynamics between the wing-body model computed by the Euler code and the wing-only model computed by the TSD code, at a 0 deg angle of attack and for Mach numbers 0.80 and 0.93. Figures 7a and 7b represent Mach 0.8 and 0.93 cases, respectively. The solid line is the original TSD result for the wing-only model. The dotted line is the Euler result for the wing-body model. The discrete points are the experimental results from [11]. The accuracy of the TSD code has already been verified in many references, such as [1,2,7–9]. For the low-Mach-number range, the surface pressure in the near-root region is slightly perturbed by the body. The results show that the fuselage affects the pressure distribution on the wing surface and the slightly-more-negative pressure coefficient distribution is analogous to the thicker airfoil result shown in Figs. 3a and 3b. That is, the aerodynamic force acting on the wing surface for the wing-body model is the same as the aerodynamic force for the somewhat-thicker airfoil wing-only model. The maximum difference in pressure coefficient in Fig. 3a of about 0.17 for the 4% thickness variation is, however, larger than the body effect shown in Fig. 7. Furthermore, the perturbed pressure distribution in the near-root region disappears in the outer spanwise regions. The pressure difference between experimental and TSD data is approximately 4 times larger than the difference between experimental and Euler results at 20% spanwise location. At 60% spanwise location, the predicted pressure difference is decreased to 1.2 times larger than the difference between experimental and Euler results. But the accuracy of TSD for wing-body model has a limited range. Actually, this wing-body model is well designed and the slim body has little influence on wing aerodynamics, and so the body effect is not that significant in this case. Moreover, Fig. 7b shows that the body effect remains enclosed between the wing root and midspan wing station. Unlike the lower Mach number case in which the perturbed pressure is uniformly distributed on the wing surface, the higher Mach number case shows that the perturbed pressure is not uniform along the chordwise axis. This means that the compressibility effect is changed along the inboard wing region.

Figure 8 shows the comparison of the steady aerodynamics between the wing-only model computed by the original TSD code and the inverse-designed TSD code at 2 deg angle of attack for Mach numbers 0.8 and 0.93. Figures 8a and 8b contain Mach number 0.8 and 0.93 cases, respectively. For the computation of the original and the corrected cases, the grid system is the same as in Fig. 6. The solid line is the inverse-designed TSD, the dotted line is the original TSD result, and the discrete points are the experimental data from [11]. The inverse-designed TSD means that it includes the body effect by using the MGM inverse design method; that is, the inverse-designed slope information at a 0 deg angle of attack is applied to the TSD code. As previously mentioned, Fig. 8a shows that the body effect is not significant, but slightly changes the pressure distribution in the near-root region. The perturbation caused by the body almost disappears as one approaches the wing tip. Nonetheless, the inverse design TSD code predicts the pressure distribution on the wing surface better than the original TSD, for Mach number 0.93. For the case with a 2 deg angle of attack, the body has an effect on the surface pressure distribution up to the midspan region. The inverse design method works well with this case in which there is an angle-of-attack variation.

To apply the inverse design method to an aeroelastic analysis, the AGARD 445.6 weakened model 3 is interpolated.

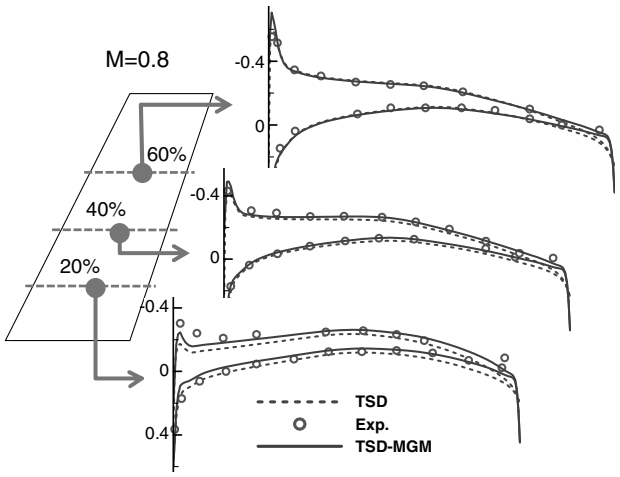

a) Mach 0.8

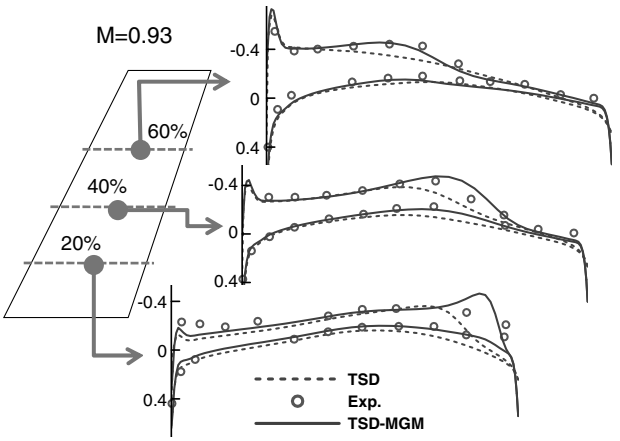

b) Mach 0.93

Fig. 8 Comparison of steady aerodynamics between original and inverse-designed TSD wing model at $M = 0.8, 0.93$ and angle of attack of 2 deg.

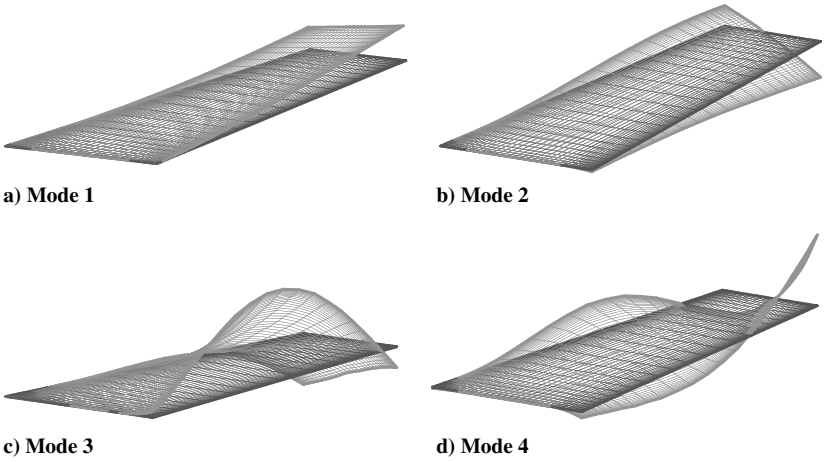

a) Mode 1 b) Mode 2

c) Mode 3 d) Mode 4

Fig. 9 AGARD 445.6 splined mode shapes.

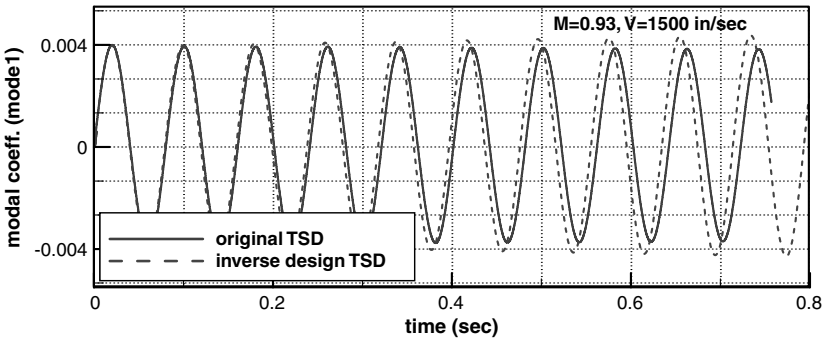

a) Time-domain analysis

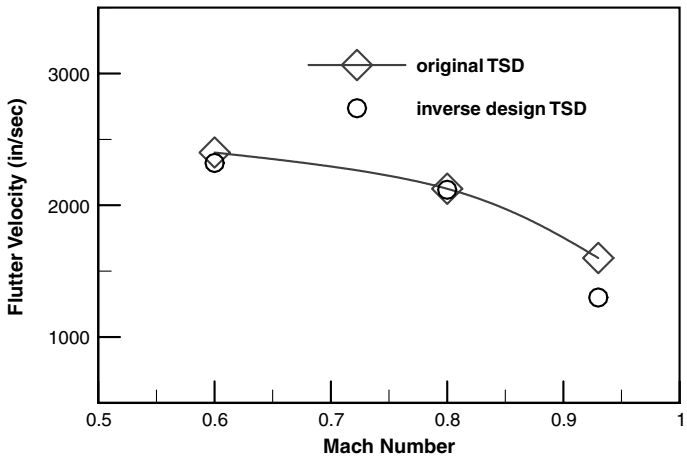

b) Flutter boundary

Fig. 10 Flutter boundary from time-domain analysis.

Figure 9 shows the mode shapes interpolated from the AGARD model with assuming the frequencies as 9.6, 38, 48, and 92 Hz. The air density is 0.000127 slug/ft^3. Figure 10 shows the flutter boundary and its time-domain analysis result. Figure 10a shows the response of the first modal coefficient. The converging solid line is from the original TSD and the diverging dotted line is from the inverse-designed TSD at $M = 0.93$ and $V = 1500$ in./s. To determine the exact flutter boundary, the moving-block method is used; Fig. 10b is the final result. The slight aerodynamic influence of the body does not show a significant change of flutter boundary in the low-Mach-number range. However, if the freestream Mach number is increased over 0.93, the body has an effect up to the midspan region. This causes the unstable structural motion and lowers the flutter stability boundary.

IV. Conclusions

In this study, an efficient aeroelastic analysis method including the body effect was presented. To apply the body effect to the TSD aeroelasticity, the MGM inverse design method was used. In the first place, the MGM inverse design method was validated by testing 2-D airfoil sections. Next, the wing-body and wing-only models were analyzed by using Euler and TSD codes, respectively, at Mach numbers 0.8 and 0.93. In the low-Mach-number range, the slight

perturbation due to the body was shown in the near-root region, but the difference was not large. For the case of Mach number 0.93, however, the body has an effect up to the midspan region. Then the inverse-designed TSD and the original TSD were compared for the case of an angle of attack of 2 deg. Present results showed that the inverse-designed TSD could predict steady pressure distributions well for the case of the angle-of-attack change. In the end, aeroelastic analyses were performed. The mild perturbation in the low-Mach-number range did not change the flutter boundary, but the strong compressibility effect at Mach number 0.93 dropped the boundary. These results were about the well-designed slim body and high-aspect-ratio wing-body model. If the cases involve missile wings, the body effect on aeroelasticity will be more significant.

Acknowledgments

This work was supported by Defense Acquisition Program Administration and Agency for Defense Development under contract UD070041AD and by the second stage of the Brain Korea 21 Project in 2009. The authors are grateful for their support.

References

[1] Kim, J. Y., Kim, K. S., Lee, I., and Park, Y. K., "Transonic Aeroelastic Analysis of All-Movable Wing with Freeplay and Viscous Effects," *Journal of Aircraft*, Vol. 45, No. 5, 2008, pp. 1820–1824. doi:10.2514/1.37435

[2] Yoo, J. H., Kim, D. H., Kwon, H. J., and Lee, I., "Nonlinear Aeroelastic Simulation of a Full-Span Aircraft with Oscillating Control Surfaces," *Journal of Aerospace Engineering*, Vol. 18, No. 3, 2005, pp. 156–167. doi:10.1061/(ASCE)0893-1321(2005)18:3(156)

[3] Lee, S. J., Im, D. K., and Lee, I., "Efficient Aerodynamic Computation of a Wing Model Considering Body Effect for the Aeroelastic Application," *KSAS International Journal* (accepted for publication).

[4] Malone, J. B., Narramore, J. C., and Sanker, L. N., "Airfoil Design Method Using the Navier–Stokes Equations," *Journal of Aircraft*, Vol. 28, No. 3, 1991, pp. 216–224. doi:10.2514/3.46015

[5] Soemarwoto, B. I., Labrujere, Th. E., Laban, M., and Yansyah, H., "Inverse Aerodynamic Shape Design for Improved Wing Buffet-Onset Performance," NLR TP-2000-150, 2000.

[6] Kim, H. J., Koc, S., and Nakahashi, K., "Surface Modification Method for Aerodynamic Design Optimization," *AIAA Journal*, Vol. 43, No. 4, 2005, pp. 727–740. doi:10.2514/1.11181

[7] Batina, J. T., "Efficient Algorithm for Solution of the Unsteady Transonic Small-Disturbance Equation," *Journal of Aircraft*, Vol. 25, No. 7, 1988, pp. 598–605. doi:10.2514/3.45629

[8] Kim, J. Y., Kim, K. S., Lee, S. J., and Lee, I., "Transonic Nonlinear Aeroelastic Analysis of Aircraft Tail Wings Using Multiblock Approach," *Journal of Aircraft*, Vol. 45, No. 4, 2008, pp. 1344–1357. doi:10.2514/1.34824

[9] Kim, D.-H., and Lee, I., "Transonic and Low-Supersonic Aerodynamic Analysis of a Wing with Underpylon/Store," *Journal of Aircraft*, Vol. 37, No. 1, 2000, pp. 189–192. doi:10.2514/2.2582

[10] Kim, H. J., and Rho, O. H., "Aerodynamic Design of Transonic Wings Using the Target Pressure Optimization Approach," *Journal of Aircraft*, Vol. 35, No. 5, 1998, pp. 671–677. doi:10.2514/2.2374

[11] Loving, D. L., and Estabrooks, B. B., "NACA Research Memorandum," NACA RM L51F07, 1951.

[12] Sung, C. H., Park, S. H., and Kwon, J. H., "Multigrid Diagonalized ADI Method for Compressible Flows," AIAA Paper 2001-2556, 2001.